A Study of the Relationship between Low-level Jet and Inversion Layer over an Agroforest Ecosystem in East China Plain①

Zhong Zhong (钟 中) and Wang Hanjie (王汉杰)

Eco-Environmental Research Center in Atmospheric Boundary Layer P. O. Box 003, Nanjing 211101

(Received March 15, 1999; revised May 25, 1999)

ABSTRACT

The relationship between the super-low-level jet (LLJ) and inversion layer over an agroforest ecosystem on the Huang-Huai-Hai plain in the eastern China is studied by means of a time-independent *K*-closure model. It is found that the intensified inversion near the surface of a luxuriantly growing agroforest ecosystem leads to the formation and development of the LLJ, the more intense the inversion, the stronger is the LLJ. The critical value of inversion intensity index for the LLJ formation is 0.75°C / 100 m, which relates to the necessary geostraphic wind velocity of 6.0 to 10 m / s at the top level of the model. The numerical calculations show that the roughness length of the underlying surface has considerable effects on the LLJ structure.

Key words: Low-level jet, Temperature inversion, Agroforest ecosystem

1. Introduction

Wind profile with the relevant low-level jet (LLJ) is one of the most important factors that characterize the structure of the atmospheric boundary layer. The LLJs were reported in Europe (Sladkovic and Kanter, 1977; Kraus et al., 1985), Africa (Anderson, 1976; Hart, et al., 1978), North America (Stull, 1988; Arritt et al., 1997), Australia (Malcher and Kraus, 1983; Garratt, 1985) and East Asia (Wang et al., 1996; Chen and Hsu, 1997). Different investigators used different criteria for identifying the LLJs. Some required wind speed greater than a particular value (e.g., 12, 16, or 20 m / s) below a specific height (e.g. 1000, 1500, or 2500 m), while others required the speed to be supergeostrophic (Stull, 1988). According to the height where the LLJs occur, we prefer to classify the LLJs into two different categories. The LLJs occurring above the 1000 m level and evidently relating to some synoptic systems are considered as the common type, which is more important to atmospheric precipitation and weather forecasting (Arritt et al., 1998). The field campaign of NOAA Profile Network (NPN) conducts hourly wind profiles to study climatology of the LLJ over the Great Plains of the United States. The peak precipitation episode of the 1993 flood is found to be associated with a sustained period of high incidence of the strong LLJ (over 20m / s) (Arritt et al., 1997). Zhong (1998) pointed out that the NPN data set permits a much more detailed picture of the Great Plains LLJ than is possible from the previous studies.

The LLJs that occur below 1000 m level, mostly below 500 m, are called

①The project was supported by the National Natural Science Foundation of China (NSFC) (49975016).

super–low–level–jet, which is evidently unrelated to synoptic systems but to the dynamic forcing on the lower boundary. These LLJs are often called nocturnal jets because they form frequently at night when the strong surface cooling causes inversion. The super–low–level–jets are not as important as the higher level ones in the synoptic scale weather forecasting, but they are more important in understanding the turbulence structure and mass and / or energy flow occurring in the atmospheric boundary layer. The present study will focus on the super–low–level–jet only though the abbreviation LLJ is also used in the text. Most of the earlier LLJ studies focused on numerical simulations (Delage, 1974; Duynkerke, 1988; Smedman et al., 1993). Delage (1974) proposed a time–dependent model with the K–closure scheme to simulate the inversion growth and the LLJ development. With the heat conservation equation included, Delage's model can be used to study the development of the nocturnal boundary layer from an initially neutral atmosphere and the relevant ground cooling. From the time–independent point of view, the present model is more like Duynkerke's (1988) model that uses the E–ε closure technique.

The East China Plain, known as the Huang (Yellow River)–Huai (Huai River)–Hai (Hai River) Plain (Zuo and Zhang, 1990), is topographically similar to the U.S. Great Plains where crops grow in an extensive scope. The reported LLJ occurrence in this area is as frequent as in the Great Plains. Yet, the East China Plain is the largest region for food, cotton and vegetable oil production in China. Under the governmental prompting and guidance, local farmers built windbreaks to protect crops from severe weathers. Getting into the 1990s, windbreaks have become the most favourable agroforest technique, and covered 86% of the arable land, as results the surface characteristics have been altered significantly as compared to the original mono–agricultural system. What happens to the low–level atmospheric circulation? Does the altered lower boundary condition affect the formation and development of the LLJ, if so, how? Proposals for studying the effect of boundary layer forcing dynamics on the Great Plains LLJ emerge on INTERNET as often as not.

Based on the intensive field radiosonde data in the central part of Huang–Huai–Hai Plain, Wang and Klaassen (1995) presented a one–dimensional prognostic model to simulate the profiles of wind, temperature and humidity. The unique feature of the model is the adjustment of the mixing length with respect to the agroforest ecosystem, later on, Wang et al. (1996) analyzed the flux–profile relations within and above this agroforest canopy according to the sonded profiles. This reveals the shortage of the one–dimensional model. Further study by Li and Wang (1997) shows that a complete three–dimensional model can simulate the wind profile much better. The present paper attempts to reveal the diagnostic relationship between the observed LLJ and the strong inversion over an agroforest ecosystem in the East China Plain. The present model is principally similar to that of Delage (1974) except for its capability of testing the effect of different inversion intensities on the LLJ formation.

2. Model description and solution to the problem

2.1 *Model description*

Under the assumption of horizontally homogeneous flow, the wind speed component u, v and the turbulent kinetic energy (E) are governed by the following equations:

$$\frac{\partial u}{\partial t} = f(v - v_g) + \frac{\partial}{\partial z}\left(K\frac{\partial u}{\partial z}\right), \tag{1a}$$

$$\frac{\partial v}{\partial t} = -f(u-u_g)+\frac{\partial}{\partial z}(K\frac{\partial v}{\partial z}) , \tag{1b}$$

$$\frac{\partial E}{\partial t} = K(S^2-\frac{g}{\theta}\frac{\partial \theta}{\partial z})+\frac{\partial}{\partial z}K\frac{\partial E}{\partial z}-\varepsilon , \tag{1c}$$

where u and v are the wind speed components in x and y directions, respectively, u_g and v_g, the geostrophic wind at the top of the model, K the eddy exchange coefficient, f the Coriolis parameter, θ the potential temperature, ε the rate of viscous dissipation of turbulent kinetic energy and

$$S^2=\left(\frac{\partial u}{\partial z}\right)^2+\left(\frac{\partial v}{\partial z}\right)^2 . \tag{2}$$

Assuming a quasi-equilibrium atmosphere with stable stratification, the time-dependent terms of Equation (1) are neglected hereinafter. For the mean velocities u and v, Equations (1a) and (1b) can be simplified as

$$-fv=-fv_g+\frac{\partial}{\partial z}\left(K\frac{\partial u}{\partial z}\right) , \tag{3a}$$

$$fu=fu_g+\frac{\partial}{\partial z}\left(K\frac{\partial v}{\partial z}\right) , \tag{3b}$$

and the turbulent kinetic energy equation is thus simply expressed as

$$\varepsilon=K(S^2-\frac{g}{\theta}\frac{\partial \theta}{\partial z}) , \tag{4}$$

where the diffusion term is also neglected in the turbulent kinetic energy equation as proposed by Wyngaard and Cote (1971).

According to the Kolmogorov's similarity theory, the following relations are used widely (Beljaars et al., 1987):

$$K=c_0 l E^{\frac{1}{2}} , \tag{5}$$

$$\varepsilon=c_0^3 E^{\frac{3}{2}} l^{-1} , \tag{6}$$

where c_0 is a constant, l is the turbulent mixing length defined by Blackadar (1962):

$$l=\kappa(Z+Z_0)[1+\kappa(Z+Z_0)\lambda_B^{-1}]^{-1} . \tag{7}$$

This definition and its various analogues are widely used in simulations (Estoque, 1973; Delage, 1974) when the atmospheric boundary layer is of stable stratification. κ in Eq.(7) is the von Karman constant, its values range over 0.35–0.41 based on Lo's summarisation (Lo, 1990). For a taller vegetation area, Businger et al. (1971) suggested a value of $\kappa=0.35$, which is used in our study because the average height of the shelterbelts was 12 m during the experimental period. Also in Equation (7), Z_0 is the roughness length for the friction of the surface, as will be seen in the following sections, it plays an important role in regulating the height and intensity of LLJ. λ_B is the value of mixing length as z approaches infinite and calculated by Blackadar (1962).

$$\lambda_B = 0.00027(u_g^2 + v_g^2)^{\frac{1}{2}} f^{-1} \quad . \tag{8}$$

From (4), (5) and (6), we have

$$K = l^2 S(1 - R_i)^{\frac{1}{2}} \quad , \tag{9}$$

where

$$R_i = \frac{\frac{g}{\theta}\frac{\partial \theta}{\partial z}}{S^2}$$

is the Richardson number, $(1 - R_i)^{\frac{1}{2}}$ represents the effects of stratification on the eddy exchange coefficient. When R_i is larger than R_{ic}, the expression of K is given by (Karlsson, 1972)

$$K = l^2 S / (1 + R_i)^2 \quad , \tag{10}$$

where R_{ic} is the critical value of R_i, it is set to be 1.0 in our studies, which assures a strong eddy exchange for a given inversion with the weak wind shear. Based on our field observation data from the agroforest area, R_i is generally less than 1.0 in the calculation of the model.

The equation set (3) is now closed by the parameterization scheme of Equation (7) through (10). The boundary conditions are set to be:

$$u = v = K = 0 \quad \text{for} \quad Z = Z_0 \quad , \tag{11a}$$

$$u = u_g, \quad v = v_g, \quad \frac{\partial K}{\partial z} = 0 \quad \text{for} \quad Z = H \quad . \tag{11b}$$

Based on the earlier study with the same data set by Wang et al. (1996), the top height (H) of the model was set to be 375 m.

2.2 *Solution to the problem*

The model atmosphere was divided into 31 layers for solving Equation set (3). The grid length was set to be unequal vertically in each of the layers, and the grids were denser at lower levels. The height of each layer was calculated by

$$Z = Z(j) = \begin{cases} 0.5j(j-1) + Z_0 \quad , & j = 1,2,3, \cdots\cdots 15 \quad , \\ Z(j-1) + 15 \quad , & j = 16,17, \cdots\cdots 31 \quad , \end{cases} \tag{12}$$

where j is the sequential number of the model layer with $j = 1$ for the ground and $j = 31$ for the top of the model. The differential expressions of Equation set (3) can be derived using the second-order non-equidistant difference scheme. The corresponding difference equations can be written as

$$\begin{aligned} -fv_j = -fv_g &+ \overline{K_j}\frac{u_{j+1} + (r-1)u_j - ru_{j-1}}{2\Delta Z_j} \\ &+ K_j\frac{u_{j+1} + ru_{j-1} - (1+r)u_j}{\Delta Z_j \Delta Z_{j-1}} \quad , \\ fu_j = fu_g &+ \overline{K_j}\frac{v_{j+1} + (r-1)v_j - rv_{j-1}}{2\Delta Z_j} \end{aligned} \tag{13}$$

$$+ K_j \frac{v_{j+1} + rv_{j-1} - (1+r)v_j}{\Delta Z_j \Delta Z_{j-1}} , \tag{14}$$

where

$$\overline{K_j} = \frac{K_{j+1} + (r-1)K_j - K_{j-1}}{2\Delta Z_j} \tag{15}$$

is the non-equidistant finite difference scheme of K in vertical, and

$$\Delta Z_j = Z(j) - Z(j-1) , \quad r = \frac{\Delta Z_j}{\Delta Z_{j-1}} . \tag{16}$$

Let $\tilde{u} = u_j$, $\tilde{v} = v_j$, the difference equations (13) and (14) can be simplified to

$$a_u \tilde{u} + a_v \tilde{v} = a_F , \tag{17a}$$

$$b_u \tilde{u} + b_v \tilde{v} = b_F , \tag{17b}$$

with

$$a_u = -\overline{K_j}(r-1)/(2\Delta Z_j) + K_j(1+r)/(\Delta Z_j \Delta Z_{j-1}) , \tag{18a}$$

$$a_v = -f , \tag{18b}$$

$$a_F = -fv_g + \overline{K_j}(u_{j+1} - ru_{j-1})/\Delta Z_j , + K_j(v_{j+1} + rv_{j-1})/(\Delta Z_j \Delta Z_{j-1}) , \tag{18c}$$

$$b_u = f , \tag{18d}$$

$$b_v = a_u , \tag{18e}$$

$$b_F = fu_g + \overline{K_j}(v_{j+1} - rv_{j-1})/\Delta Z_j + K_j(v_{j+1} + rv_{j-1})/(\Delta Z_j \Delta Z_{j-1}) . \tag{18f}$$

Equation (17) can be solved iteratively with following iterating expressions

$$u_j^{(n+1)} = u_j^{(n)} + \mu R_u^{(n)} , \tag{19a}$$

$$v_j^{(n+1)} = v_j^{(n)} + \mu R_v^{(n)} , \tag{19b}$$

where μ is the relaxation coefficient, and the superscript n represents the iteration number, and

$$R_u^{(n)} = \tilde{u} - u_j^{(n)} , \tag{20a}$$

$$R_v^{(n)} = \tilde{v} - v_j^{(n)} , \tag{20b}$$

with

$$\tilde{u} = \frac{\begin{vmatrix} a_F & a_v \\ b_F & b_v \end{vmatrix}}{\Delta} , \quad \tilde{v} = \frac{\begin{vmatrix} a_u & a_F \\ b_u & b_F \end{vmatrix}}{\Delta} , \tag{21}$$

and

$$\Delta = \begin{vmatrix} a_u & a_v \\ b_u & b_v \end{vmatrix}. \tag{22}$$

For a given temperature profile and an arbitrary initial distribution of u and v, Equation (19) can be solved iteratively until the residues of u and v are less than the pre-assigned accuracy. In this study the accuracy level was set to be 0.1 m/s for both u and v.

3. Results and discussions

3.1 *Experimental site and field observations*

The field radiosonding was conducted in the central part of the Huang-Huai-Hai Plain in the eastern China (33.7°N, 116.0°E). Over several hundred kilometres around the sounding site, the windbreaks have constructed a rather homogeneous system (Fig. 1). The forest network consists of main belts of poplar (*Popalus euramerican*) and oriental arborvitae (*P. Orientails*) and sub-belts of poplar (*P. euramericam*), Chinese berry (*Melia Azedarach*) and false indigo (*Indigofera pseudofinctoria*). The distance between main belts is 150 m and that between sub-belts is 135 m (see Fig. 1). The average height of the windbreaks which consist mainly of poplars is 12 m during the field observation. Wang and Klaassen (1995) and Wang et al. (1996) gave more details about the nature of the windbreaks.

The radiosondes were launched at a 3-hour interval from 14:00 BST, April 24 to 08:00, April 28, 1992. During the field operation, the winter wheat was at its heading/milking stages, and the forest belts (*P. euramerican*) were approximately in the middle of the leafing stage. Based on the *in situ* measurements, the green leaf area index (LAI) was approximately 5.6. More details about the field operation and the characteristics of the sounding profiles were discussed by Wang et al. (1996).

3.2 *The inversion layer structure and the LLJ formation*

The observed profiles in the clear night demonstrate that the inversion layer was formed around the midnight and maintained till the morning. The LLJ remained evident until

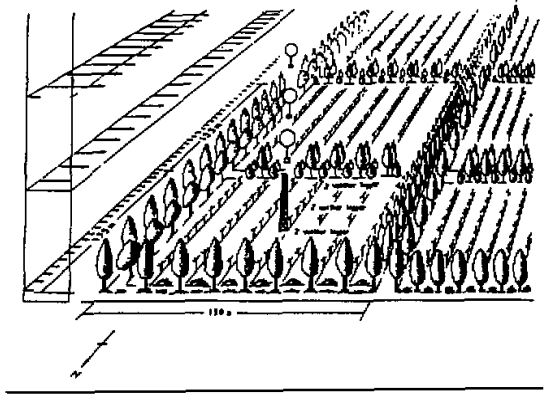

Fig. 1. Sketch of the experimental site and observation facilities.

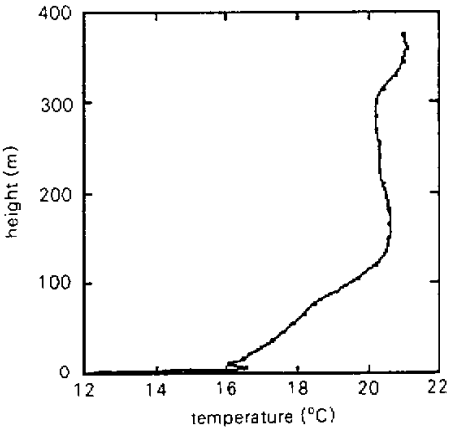

Fig. 2. Temperature profile observed at 23:00 BST, April 23, 1992.

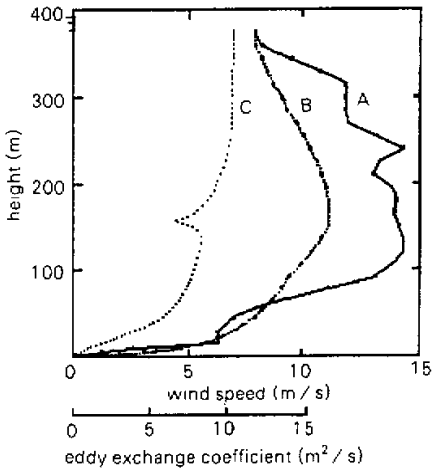

Fig. 3. Observed (line A) and calculated (line B) wind profiles and the distribution of eddy exchange coefficient (line C).

08:00 a.m. in some cases (Wang et al., 1996). Figure 2 gives the temperature profile at 23:00 BST, April 23, 1992, which represents the typical inversion feature during the observation in late April. The top of strong inversion reached 150 m , above this level, temperature was kept almost unchanged. The temperature profile shows a very stable atmospheric stratification. Let I_s denote the average inversion intensity index, and we get

$$I_s = \frac{T_t - T_s}{Z_t - Z_0} \quad , \tag{23}$$

where T_s and T_t are temperature on ground and at the top of the inversion layer respectively, Z_0 is the roughness length and Z_t is the height of inversion layer. According to Equation (23), the profile in Fig. 2 implies an inversion intensity index of about 3.0°C / 100 m below the height of Z_t.

Figure 3 presents the wind profiles (dashed line B) from the numerical model based on the observed temperature inversion index shown in Fig. 2. The roughness length was assumed to be 0.25 m according to Wang and Klaassen (1995). The observed wind speed at the top of the model was used as the upper boundary condition. For comparison, the observed wind profile (solid line A) is also shown in the same figure. The observed profile shows a super–geostrophic feature above the 60 m height, where the LLJ is around 135 m level, and the maximum wind speed is 14 m / s, about 75% greater than the geostrophic wind of 7.9 m / s at the top of the model. For the calculated wind profile, however, the super–geostrophic wind is found above 60 m from ground, which agrees with the observations, but the jet is around 150 m, slightly higher than the observed one. The calculated wind speed and its maximum value are lower than the observations. Line C in Fig. 3 denotes the vertical distribution of the eddy diffusion coefficient, the non–continuous singular point occurs at the height of LLJ. The wind spirals that show the change of the wind direction are illustrated in Fig. 4.

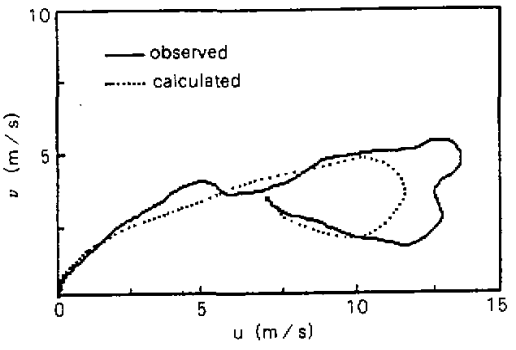

Fig. 4. Observed (solid line) and calculated (dotted line) wind spirals.

It has been found that the wind direction changes at the approximate same height for both calculated (dotted) and observed (solid) spirals.

By comparing the observed and calculated three-dimensional structures from Fig. 3 and Fig. 4, one can see that the simple model described in Section 2 is able to illustrate the formation of the LLJ corresponding to a particular inversion status in the atmospheric boundary layer. It seems certain that, whenever the inversion intensity index exceeds the critical value, the super-geostrophic LLJ occurs. Based on the numerical calculations (see next section), the height and the intensity of the jet will experience some variation as the inversion index changes. In this agroforested area, the radiation cooling layer is thicker than that in the vegetation-free areas. The inversion is intensified in night hours because of the underneath cooling, which stimulates the formation and development of the LLJ. The observations in the Great Plains by Ogawa et al. (1982) and Lenschow et al. (1988) revealed that the LLJ always co-exists with inversion.

3.3 *The model sensitivity study*

3.3.1 *The effects of inversion intensity*

Theoretically, the inversion intensity will affect both the strength and the height of an LLJ because of the thermal wind mechanism. Keeping other model parameters unchanged, the wind profiles were calculated in virtue of different inversion intensities for the model sensitivity test. Let T_s and $T(z)$ represent the temperature on the surface and at height z respectively, we have

$$\Delta T(z) = T(z) - T_s \ . \tag{24}$$

The temperature distribution in z direction is expressed as

$$T(z) = T_s + \alpha \Delta T(z) \ , \tag{25}$$

where α is an adjusting factor for the inversion intensity, with $\alpha = 1$ denoting the observed temperature distribution, and $\alpha < 1$ (> 1) the less (more) intense inversion. Figure 5 shows the wind profiles calculated for different α. The wind speed increases slowly from the ground to the model top without reference to super-geostrophic component when α is less than 0.25, which corresponds to an inversion intensity of less than 0.75°C/ 100 m. On the other hand,

for $\alpha = 0.25$, the wind velocity below the model top is greater than the geostrophic wind, and the LLJ appears in all cases with α larger than 0.25. For example, for $\alpha = 2.0$, which corresponds to a mean inversion intensity of 6.0°C / 100 m, the maximum wind velocity in the jet is about 22 m / s. In general, the jet height is lower than the height of the inversion layer. Figure 5 demonstrates a close relationship between an LLJ and an inversion layer in the atmospheric boundary layer. It appears that the more intense the inversion, the stronger is the LLJ. A critical inversion intensity index of about 0.75°C / 100 m came from the repeated calculations.

Based on the radiosonde profiles, the near surface inversion layer formed after 20:00 BST and reached its most intense level from 02:00 to 05:00 BST of the day. At the same time, the LLJ formed gradually and reached its highest intensity in the early morning (Wang et al., 1996). After sunrise, the inversion layer was disturbed first from the bottom due to the solar radiation heating and did not disappear completely until 10:00 BST in this luxuriant vegetation area. The LLJ showed similar diurnal course to that of the inversion.

Observations by Rowe et al. (1982) suggested that no LLJ formed in the absence of an inversion layer, a statement that fully supports our simulations. However, by examining the "wind defect" between the actual wind and the geostrophic wind, Duynkerke (1988) found that the LLJ formed when the inversion was very weak. This suggests that the inversion is not the only factor in stimulating the LLJ formation. Delage (1974) also found that the increased intensity of inversion relates to the decrease of LLJ strength. Arritt and Segal (1998) argued recently that the LLJ genesis requires the combination of a strong geostrophic flow with the ageostrophic boundary-layer forcing. The following section will be devoted to the effects of the geostrophic wind at the model top and the underlying frictional forcing on the structure of LLJ in our special agroforest area.

3.3.2 *The effects of geostrophic forcing*

The geostrophic wind at the model top was used as the upper boundary condition in the model. Surely, it has some influence on the simulated wind profile and hence on the formation and structure of LLJ. We use the following equation to set up different upper boundary conditions

$$u'_g = \beta u_g, \quad v'_g = \beta v_g \ . \tag{26}$$

By using the observed temperature profiles, the model was run in different cases, as shown in Fig. 6. Under the conditions of the selected values of β, an LLJ appeared only for $\beta = 0.75$, 1.0 and 1.25. It is obvious that the larger the β, the less is the super-geostrophic wind component and the higher (H_c) is the LLJ. For example, $H_c = 95$ m for $\beta = 0.75$, and $H_c = 270$ m for $\beta = 1.25$. Neither a very small $\beta (< 0.5)$, nor a large one ($\beta > 1.5$) can form the significant super-geostrophic LLJ. So the conclusion is that, besides the effects of temperature inversion, the intensity of geostrophic forcing at the top of the model also plays an important role in the formation of LLJ. Based on the analysis of the field observational wind profiles and the calculated ones according to the assigned typical temperature profile, we obtained the critical values of the geostrophic wind from 6.0 m / s to 10 m / s at the model top that was responsible for the LLJ formation. This should be considered in the conventional LLJ prediction. So far few researches have been done on the effect of the geostrophic wind at the top of the boundary layer on the structure and strength of the LLJ. As a matter of fact, the so-called geostrophic flow or geostrophic forcing exists all the time. The simulations will be in better agreement with the observations if the vertical or time-dependent variation of the pressure gradient is included in the model.

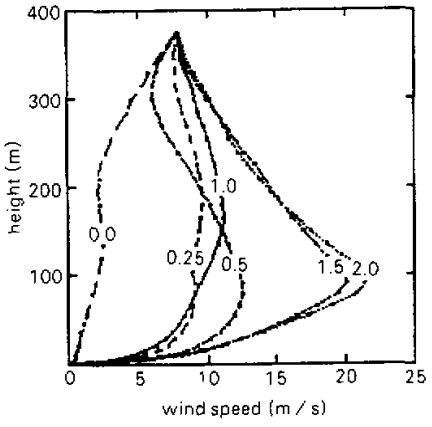

Fig. 5. Wind profiles for different values of α.

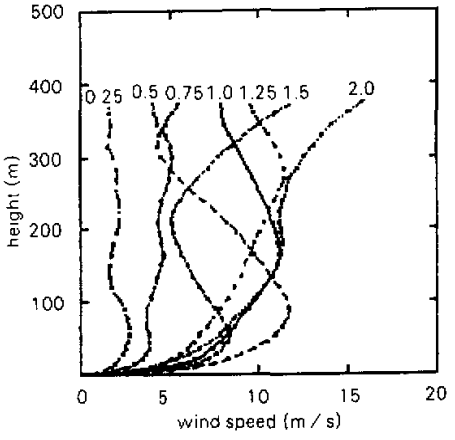

Fig. 6. wind profiles for different values of β.

3.3.3 *The effect of roughness length*

It has been pointed out that the roughness length affects the distribution of the wind profile in the boundary layer, especially of the tall vegetation areas (Wang and Klaassen, 1995). Since the experimental site is in an agroforested area, the average height of the forest belts was about 12 m at the experimental time, the effect of the roughness length needs to be studied further. Figure 7 shows the wind profiles calculated with different values of the roughness length Z_0, when the temperature distribution and the geostrophic forcing were kept constant as done in Section 3.2. The wind speed close to the surface increased rapidly and the LLJ appeared at 75 m for $Z_0 = 0.01$ m. The very small Z_0 represents the newly ploughed farmland or city lawns. Because the wind speed decreased rapidly above the jet and the minimum was at a height of 250 m, the wind shear in vertical was significant. The LLJ height rose to a higher level and the super-geostrophic wind decreased as Z_0 become larger. A larger Z_0 corresponds to a slower wind speed increasing with height and *vice versa*. The height of the LLJ is in a range of 200–300 m when $0.50\ \text{m} < Z_0 < 1.0$ m, a fact that is in agreement with the observed wind profiles and the roughness length of the agroforested area. It has been demonstrated in the previous studies (Wang and Klaassen, 1995; Wang et al., 1996) that the roughness length in the study area varies from 0.5 m to 1.2 m and the LLJs develop around 250 m, depending on the atmospheric stability. Delage (1974) also examined the relationship between the height of the LLJ and the roughness length Z_0, stating that the decrease of the surface Rossby number $R_0 (= \frac{G}{Z_0 f})$, which means the increase of Z_0 will lead to the increase of the inversion thickness and finally the LLJ lifting.

4. Conclusions

Based on the radiosonde data in an agroforested area, the relationship between the LLJ formation and various thermodynamic characteristics in the atmospheric boundary layer, such as the inversion intensity, the geostrophic forcing, and the roughness length, was

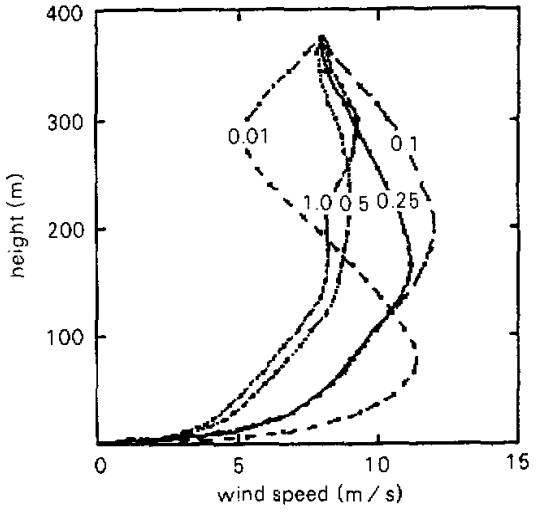

Fig. 7. Wind profiles for different values of Z_0.

investigated using a simple closure technique in the boundary layer meteorology. It is found that the formation and the maintenance of the temperature inversion caused by the intensified long-wave radiation cooling of the vegetative canopy at night is a principal factor, but not the unique one, for the LLJ formation. The stronger the temperature inversion, the more intense is the LLJ. Besides the inversion intensity, both the geostrophic forcing at the top level of the model and the roughness length of the underlying surface affect the strength and the height of LLJ effectively.

The LLJ is important in regulating the turbulence structure and then affecting the transfer of momentum, heat, water vapour, and other trace gasses between the biosphere and the low level atmosphere. It is worthwhile to study its relation to any specific terrestrial ecosystem, especially for those with tall vegetation, like the forest or agroforested ecosystems. In a dense forest or agroforest area, because of the ground roughness, the frictional forcing increases, and so do the degree of supergeostrophic wind and the height of LLJ. All these factors should be included in the LLJ study, which will contribute to the LLJ prediction and to our understanding of the interaction between the biosphere and the atmosphere.

REFERENCES

Anderson, D. L. T., 1976: The low-level jet as a western boundary current. *Mon. Wea. Rev.*, **104**, 907–921.

Arritt, R. W., T. D. Rink, M. Segal, D. P. Todey, C. A. Clark, M. Mitchel, and K. M. Labas, 1997: The Great Plains Low-level jet during the warm season of 1993. *Mon. Wea. Rev.*, **125**, 2176–2192.

Arritt, R. W., and M. Segal, 1998: Overview of JETEX-97. Presented on the INTERNET with a website of http: / / www.mesoscale.iastate.edu / jetexhtm.htm.

Beljaars, A. C. M., J. L. Walmsley, and P. A. Taylor, 1987: A mixed spectral finite-difference model for neutrally stratified boundary layer flow over roughness changes and topography. *Bound. Layer Meteor.*, **38**, 273–303.

Blackadar, A. K., 1962: The vertical distribution of wind turbulence exchange in a neutral atmosphere. *J. Geophys.*

Res., **67**, 3095–3102.

Businger, J. A., J. C. Wyngaard, Y. Izumi, and E. F. Bradley, 1971: Flux–profile relationship in the atmospheric surface layer. *J. Atmos. Sci.* **28**, 181–189.

Chen G., Taien, and Yingshao Hsu, 1997: Composite structure of a low–level jet over southern China observed during the TAMEX. *J. Meteor. Soc. Japan*, **75**, 1003–1018.

Delage, Y., 1974: A numerical study of the nocturnal atmospheric boundary layer. *Quart. J. Roy. Meteor. Soc.*, **100**, 351–364.

Duynkerke, P. G., 1988: Application of $E-\varepsilon$ turbulence closure model to the neutral and stable atmospheric boundary layer. *J. Atmos. Sci.*, **45**, 865–880.

Estoque, M. A., 1973: Numerical modelling of the planetary boundary layer, In: D. A. Haugen (Editor), Workshop on Micrometeorology. *American Meteor. Soc.*, Boston, USA 217–720.

Garratt, J. R., 1982: Observations in the nocturnal boundary layer. *Bound. Layer Meteor*, **22**, 24–48.

Garratt, J. R., 1985: Inland boundary layer at low latitudes. Part I, the nocturnal jet. *Bound. layer Meteor.*, **32**, 307–327.

Hart, J. E., G. V. Rao, H. Van de Boogaard, J. A. Young, and J. Findlater, 1978: Aerial observations of the African low–level jet stream. *Mon. Wea. Rev.*, **106**, 1714–1724.

Karlsson, E., 1972: A numerical model for the boundary layer of the atmosphere at neutral and stable stratification. DM–7, Inst. of Meteorology, University of Stockholm 26–53.

Kraus, H., J. Malcher, and E. Schaller, 1985: Nocturnal low–level jet during PUKK. *Bound. Layer Meteor.*, **31**, 187–195.

Lenschow, D. H., Li Xingsheng, Zhu Cuijuan, and B. B. Stankov, 1988: The stable stratified boundary layer over the Great Plains. *Bound. layer Meteor*, **42**, 95–121.

Li, Xunqiang, and Wang Hanjie, 1977: A boundary layer meteorological model and its application in agroforestry study. In Chao Chison (ed.). *Forest and Environment–Research and Practice*, China Forestry Publishing House, 163–178.

Lo, A. K., 1990: On the determination of zero–plane displacement and roughness length for flow over forest canopies. *Bound. layer Meteor*, **51**, 255–268.

Malcher, J., and H. Kraus, 1983: Low–level jet phenomena described by an integrated dynamic PBL model. *Bound. layer Meteor*, **27**, 327–343.

Ogawa, Y., and T. Ohara, 1982: Observation of the turbulent structure in the planetary boundary layer with a kytoon–mounted ultrasonic anemometer system. *Bound. Layer Meteor.*, **22**, 123–131.

Rowe, R. D., S. F. Benjamin, and K. P. Chung, 1982: Tetroon flights across a ridge. *Bound. Layer Meteor*, **23**, 161–173.

Sladkovic, R., and H. J. Kantor, 1977: Low–level jet in the Bavarian pre–alpine regime. *Arch. Meteor. Geophys. Bioklimatol., Ser. A* **25**, 343–355.

Smedman, A–S., M. Tjernstrm, and U. Hogstroem, 1993: Analysis of the turbulence structure of a marine low–level jet. *Bound. Layer Meteor.* **66**, 105–126.

Stull, R. B., 1988: *An Introduction to Boundary Layer Meteorology*, Kluwer Academic publishers, Dordrecht, 520–527 666 pp.

Wang, H., G. Xie, and Y. Fang, 1996: Structure and diurnal variations of the ecoboundary layer in a checkerboard agroforestry system in the East China Plain', In: Hsiung Wenyu and Paul F. Chandler (Editors). *Agroforestry Research and Practice*, China Forestry Publishing House, Beijing, 301–313.

Wang, H., and W. Klaassen, 1995: The surface layer above a landscape with a rectangular windbreak system. *Agricultural and Forestry Meteorology*, **72**, 195–211.

Wyngaard, J. C., and O. R. Cote, 1971: The budgets of turbulent kinetic energy and temperature variance in the atmospheric surface layer. *J. Atmos. Sci.*, **28**, 190–201.

Zhong, S., 1998: Great plains low–level jet, Presented on the INTERNET with a website of http:/ / www.pnl.gov / atmos sciences / as meso4.html.

Zuo, D., and P. Zhang, 1990: The Huang–Huai–Hai Plain. In *The Earth as Transformed by Human Action*, B. L. Turner II and W. C. Clark (Editors), Cambridge University Press, Cambridge, 473–477.